COBEM 2021 26th International Congress of Mechanical Engineering
November 22-26, 2021, Virtual Congress, Brazil

COB-2021-0402
CHAOS AND HYPERCHAOS IN A TWO-DEGREE OF FREEDOM DUFFING OSCILLATOR

Luã Guedes Costa
Marcelo Amorim Savi
Universidade Federal do Rio de Janeiro – COPPE – Department of Mechanical Engineering Center for Nonlinear Mechanics – MECANON – Rio de Janeiro – RJ – Brazil – 21.941.972
guedes@mecanica.coppe.ufrj.br, savi@mecanica.ufrj.br

Luciana Loureiro da Silva Monteiro
Centro Federal de Educação Celso Suckow da Fonseca - CEFET/RJ - Mechanical Engineering Graduate Program - 229 Maracanã Av. - Rio de Janeiro - RJ - Brazil - 27271-110
luciana.monteiro@cefet-rj.br

Abstract. *The classical Duffing oscillator is often used to describe a great variety of physical phenomena. A deep nonlinear dynamics investigation of these systems is important to understand the nuances of the involved phenomena and their applications. This contribution deals with a parametric analysis of a two-degree of freedom Duffing oscillator. Stiffness coefficients are investigated for different stability configurations of the system. Besides, the external forcing parameters are also evaluated mapping and quantifying different types of responses. Numerical simulations are employed using fourth order Runge-Kutta method. Poincaré sections and Lyapunov exponents are employed to define different kinds of responses, characterizing periodic, chaotic and hyperchaotic behaviors. Results show a variety of complex behaviors associated with these types of systems.*

Keywords: *Nonlinear Dynamics, Duffing Oscillator, Chaos, Lyapunov Exponents, Multiple DoF Systems.*

1. INTRODUCTION

The Duffing Oscillator was first described by the German engineer Georg Duffing (1918). In general, Duffing-type systems may exhibit periodic and chaotic motion, and a vast open literature is dedicated to cover its main characteristics. These kind of systems are often employed to represent specific mechanical and electrical nonlinear systems, establishing experimental basis for different kinds of investigations. Common examples are the dynamical characterization of the magnetoelastic beam structure, initially investigated by Moon and Holmes (1979) and later by Hikihara and Kawagoshi (1996), and Tam and Holmes (2014); the Duffing-type experimental nonlinear circuit investigated by Fouda *et al.* (2016); the experimental display that mimics a Duffing system developed by Gottwald *et al.* (1992). Duffing-type systems have also been employed in emergent research fields as energy harvesting systems (Erturk and Inman, 2011; Masana and Daqaq, 2011; Paula *et al.*, 2015; Costa *et al.*, 2021) and message encryption for secure communications using chaotic attractors (Zaher, 2018).

The versatility of the simple mathematical model of the Duffing oscillator represented by its wide range of applications justifies the need to further investigate its characteristics on systems with multiple degrees of freedom. In addition, a literature review shows few texts dealing with the subject. Natsiavas and Hagler (1991) showed multiple solution branches of a 2 degree of freedom duffing oscillator utilizing the method of trigonometric collocation along with Floquet theory. Savi and Pacheco (2002) investigated the transmissibility between two coupled Duffing oscillators; Kenfack (2003) revealed the bifurcations characteristics of two-coupled double-well Duffing oscillators and found the presence of sudden chaos and mostly Hopf bifurcations; Musielak *et al.* (2005) studied chaotic behavior and routes to chaos in a multi degree of freedom Duffing system.

The continuous effort to map and quantify periodic and aperiodic behaviors of Duffing-like systems (Zeni and Gallas, 1995; Costa *et al.*, 2019) is important to determine the best configurations for different kinds of application. This work addresses a parametric investigation of a two-degree of freedom oscillator in order to map and quantify different kinds of dynamical responses for different stability conditions. Steady state numerical solutions are determined using fourth order Runge-Kutta method. Periodic, chaotic and hyperchaotic behaviors are classified by the employment of Poincaré Maps and the estimation of Lyapunov Exponents by the method proposed by Wolf *et al.* (1985).

2. PHYSICAL MODELING

Consider the mechanical representation of a two-degree of freedom oscillator, depicted in Figure 1, consisted of two masses, m_i $(i = 1, 2)$, supported by two nonlinear springs with a restitution force f_i $(i = 1, 2)$ and linear viscous dampers with coefficient c_i $(i = 1, 2)$. The system is subjected to a harmonic excitation $F_i(t)$.

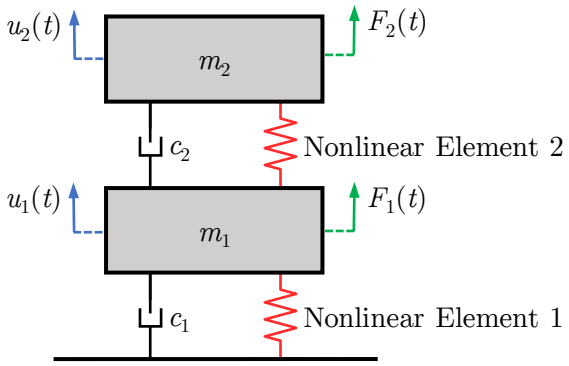

Figure 1: Mechanical lumped model representation of a two-degree of freedom Duffing oscillator.

The Duffing-type restitution forces of the nonlinear elements are typically represented by a cubic polynomial behavior as follows:

$$f_1(u_1) = (k_1 + a_1)u_1 + b_1 u_1^3 \tag{1}$$
$$f_2(u_2 - u_1) = (k_2 + a_2)(u_2 - u_1) + b_2(u_2 - u_1)^3 \tag{2}$$

By establishing the equilibrium of the system, the dynamical equations of motion can be expressed as follows, where it is assumed a harmonic excitation of the form: $F_1(t) = A\sin(\omega t)$ and $F_2(t) = 0$,

$$m_1 u_1'' + c_1 u_1' - c_2(u_2' - u_1') + (k_1 + a_1)u_1 + b_1 u_1^3 - (k_2 + a_2)(u_2 - u_1) - b_2(u_2 - u_1)^3 = A\sin(\omega t) \tag{3}$$
$$m_2 u_2'' + c_2(u_2' - u_1') + (k_2 + a_2)(u_2 - u_1) + b_2(u_2 - u_1)^3 = 0 \tag{4}$$

where $k_i (i = 1, 2)$ are the linear stiffness of the respective degree of freedom, and $a_i (i = 1, 2)$ and $b_i (i = 1, 2)$ are the Duffing stiffness coefficients. Subscript $()' = d()/dt$ represents the time derivative.

A dimensionless approach is now in focus by defining $\omega_1 = \sqrt{k_1/m_1}$ and $\omega_2 = \sqrt{k_2/m_2}$ as the reference frequencies around one stable equilibrium point for the first and second degrees of freedom of the system, respectively; and considering a reference length (L), the dimensionless time and displacements are given by:

$$\tau = \omega_1 t, \qquad x_1 = \frac{u_1}{L}, \qquad x_2 = \frac{u_2}{L} \tag{5}$$

Thus, through the chain rule, one can determine the dimensionless variables:

$$\dot{x}_1 = \frac{u_1'}{\omega_1 L}, \qquad \ddot{x}_1 = \frac{u_1''}{\omega_1^2 L}, \qquad \dot{x}_2 = \frac{u_2'}{\omega_1 L}, \qquad \ddot{x}_2 = \frac{u_2''}{\omega_1^2 L} \tag{6}$$

where $\dot{()} = d()/d\tau$ represents the dimensionless time derivative. Therefore, Equations 3 and 4 can be rewritten in dimensionless form as:

$$\ddot{x}_1 + 2\zeta_1\dot{x}_1 - 2\zeta_2(\dot{x}_2 - \dot{x}_1) + \alpha_1 x_1 + \beta_1 x_1^3 - \alpha_2(x_2 - x_1) - \beta_2(x_2 - x_1)^3 = \gamma\sin(\Omega\tau) \tag{7}$$
$$\ddot{x}_2 + \frac{2\zeta_2}{\rho}(\dot{x}_2 - \dot{x}_1) + \frac{\alpha_2}{\rho}(x_2 - x_1) + \frac{\beta_2}{\rho}(x_2 - x_1)^3 = 0 \tag{8}$$

where the dimensionless parameters are:

$$\zeta_1 = \frac{c_1}{2\omega_1 m_1}, \qquad \zeta_2 = \frac{c_2}{2\omega_1 m_1}, \qquad \bar{\alpha}_1 = \frac{a_1}{\omega_1^2 m_1}, \qquad \bar{\alpha}_2 = \frac{a_2}{\omega_1^2 m_1}, \qquad \beta_1 = \frac{b_1 L^2}{\omega_1^2 m_1}, \qquad \beta_2 = \frac{b_2 L^2}{\omega_1^2 m_1} \tag{9}$$

$$\gamma = \frac{A}{\omega_1^2 L m_1}, \qquad \Omega = \frac{\omega}{\omega_1}, \qquad \rho = \frac{m_2}{m_1}, \qquad \delta = \frac{\omega_2}{\omega_1}, \qquad \alpha_1 = 1 + \bar{\alpha}_1, \qquad \alpha_2 = \delta^2 \rho + \bar{\alpha}_2 \tag{10}$$

Therefore, the equations of motion can be written as follows in the canonical form,

$$\dot{\mathbf{x}} = \mathbf{f}(\mathbf{x}) \tag{11}$$

where the state variables are given by,

$$\mathbf{x} = \begin{bmatrix} x_1 \\ \dot{x}_1 \\ x_2 \\ \dot{x}_2 \end{bmatrix} \tag{12}$$

$$\mathbf{f}(\mathbf{x}) = \begin{bmatrix} \dot{x}_1 \\ \gamma \sin(\Omega\tau) - 2\zeta_1 \dot{x}_1 + 2\zeta_2(\dot{x}_2 - \dot{x}_1) - \alpha_1 x_1 - \beta_1 x_1^3 + \alpha_2(x_2 - x_1) + \beta_2(x_2 - x_1)^3 \\ \dot{x}_2 \\ -\dfrac{2\zeta_2}{\rho}(\dot{x}_2 - \dot{x}_1) - \dfrac{\alpha_2}{\rho}(x_2 - x_1) - \dfrac{\beta_2}{\rho}(x_2 - x_1)^3 \end{bmatrix} \tag{13}$$

3. STABILITY ANALYSIS

The equilibrium configurations of the system can be determined when both velocity and acceleration are zero in a non-forced system ($\gamma \sin(\Omega\tau) = 0$). Therefore, solving $\dot{\mathbf{x}} = \mathbf{f}(\mathbf{x}) = 0$ yields up to 9 equilibrium points.

$$\mathrm{EP}_1 = (\bar{x}_1, \dot{\bar{x}}_1, \bar{x}_2, \dot{\bar{x}}_2)_1 = (0, 0, 0, 0) \tag{14}$$

$$\mathrm{EP}_2 = (\bar{x}_1, \dot{\bar{x}}_1, \bar{x}_2, \dot{\bar{x}}_2)_2 = \left(0, 0, \frac{i\sqrt{\alpha_2}}{\sqrt{\beta_2}}, 0\right) \tag{15}$$

$$\mathrm{EP}_3 = (\bar{x}_1, \dot{\bar{x}}_1, \bar{x}_2, \dot{\bar{x}}_2)_3 = \left(0, 0, -\frac{i\sqrt{\alpha_2}}{\sqrt{\beta_2}}, 0\right) \tag{16}$$

$$\mathrm{EP}_4 = (\bar{x}_1, \dot{\bar{x}}_1, \bar{x}_2, \dot{\bar{x}}_2)_4 = \left(\frac{i\sqrt{\alpha_1}}{\sqrt{\beta_1}}, 0, \frac{i\sqrt{\alpha_1}}{\sqrt{\beta_1}}, 0\right) \tag{17}$$

$$\mathrm{EP}_5 = (\bar{x}_1, \dot{\bar{x}}_1, \bar{x}_2, \dot{\bar{x}}_2)_5 = \left(-\frac{i\sqrt{\alpha_1}}{\sqrt{\beta_1}}, 0, -\frac{i\sqrt{\alpha_1}}{\sqrt{\beta_1}}, 0\right) \tag{18}$$

$$\mathrm{EP}_6 = (\bar{x}_1, \dot{\bar{x}}_1, \bar{x}_2, \dot{\bar{x}}_2)_6 = \left(\frac{i\sqrt{\alpha_1}}{\sqrt{\beta_1}}, 0, \frac{i\sqrt{\alpha_2}}{\sqrt{\beta_2}} + \frac{i\sqrt{\alpha_1}}{\sqrt{\beta_1}}, 0\right) \tag{19}$$

$$\mathrm{EP}_7 = (\bar{x}_1, \dot{\bar{x}}_1, \bar{x}_2, \dot{\bar{x}}_2)_7 = \left(\frac{i\sqrt{\alpha_1}}{\sqrt{\beta_1}}, 0, -\frac{i\sqrt{\alpha_2}}{\sqrt{\beta_2}} + \frac{i\sqrt{\alpha_1}}{\sqrt{\beta_1}}, 0\right) \tag{20}$$

$$\mathrm{EP}_8 = (\bar{x}_1, \dot{\bar{x}}_1, \bar{x}_2, \dot{\bar{x}}_2)_8 = \left(-\frac{i\sqrt{\alpha_1}}{\sqrt{\beta_1}}, 0, \frac{i\sqrt{\alpha_2}}{\sqrt{\beta_2}} - \frac{i\sqrt{\alpha_1}}{\sqrt{\beta_1}}, 0\right) \tag{21}$$

$$\mathrm{EP}_9 = (\bar{x}_1, \dot{\bar{x}}_1, \bar{x}_2, \dot{\bar{x}}_2)_9 = \left(-\frac{i\sqrt{\alpha_1}}{\sqrt{\beta_1}}, 0, -\frac{i\sqrt{\alpha_2}}{\sqrt{\beta_2}} - \frac{i\sqrt{\alpha_1}}{\sqrt{\beta_1}}, 0\right) \tag{22}$$

The existence of an equilibrium point depends on the combination of the parameters α_1, α_2, β_1, β_2. EP_1 always exists; EP_2 and EP_3 exist if $\mathrm{sgn}(\alpha_2) \neq \mathrm{sgn}(\beta_2)$; EP_4 and EP_5 exist if $\mathrm{sgn}(\alpha_1) \neq \mathrm{sgn}(\beta_1)$; EP_6, EP_7, EP_8 and EP_9 exist if $\mathrm{sgn}(\alpha_1) \neq \mathrm{sgn}(\beta_1)$ and $\mathrm{sgn}(\alpha_2) \neq \mathrm{sgn}(\beta_2)$.

The nature of stability of each equilibrium point can be determined evaluating the solution through a linearization of the system around each equilibrium point. By considering the Jacobian matrix $\mathbf{J}$ evaluated at each the equilibrium point, and through its eigenvalues λ^{e}, the stability characteristics of these points are determined. On this basis, the eigenvalue spectrum of $\mathbf{J}$ can be classified in 3 sets: (1) Stable if $\{\lambda^{\mathrm{e}} \in \mathbb{C} \mid \mathrm{Re}(\lambda^{\mathrm{e}}) < 0\}$, (2) Unstable if $\{\lambda^{\mathrm{e}} \in \mathbb{C} \mid \mathrm{Re}(\lambda^{\mathrm{e}}) > 0\}$, and (3) Center if $\{\lambda^{\mathrm{e}} \in \mathbb{C} \mid \mathrm{Re}(\lambda^{\mathrm{e}}) = 0\}$.

The stability of the linearized system at the vicinity of an equilibrium point corresponds to the stability of the associated nonlinear system, as long as that point is hyperbolic, which means that the Jacobian Matrix $\mathbf{J}$ has no eigenvalue that the real part vanishes ($\mathrm{Re}(\lambda_k^{\mathrm{e}}) \neq 0, \forall k$) (Savi, 2017). The Jacobian matrix of the Duffing system is given by:

$$\mathbf{J} = \nabla^{\mathrm{T}}\mathbf{f}(\bar{x}_1, \dot{\bar{x}}_1, \bar{x}_2, \dot{\bar{x}}_2) = \begin{bmatrix} \frac{\partial \dot{x}_1}{\partial \bar{x}_1} & \frac{\partial \dot{x}_1}{\partial \dot{\bar{x}}_1} & \frac{\partial \dot{x}_1}{\partial \bar{x}_2} & \frac{\partial \dot{x}_1}{\partial \dot{\bar{x}}_2} \\ \frac{\partial \ddot{x}_1}{\partial \bar{x}_1} & \frac{\partial \ddot{x}_1}{\partial \dot{\bar{x}}_1} & \frac{\partial \ddot{x}_1}{\partial \bar{x}_2} & \frac{\partial \ddot{x}_1}{\partial \dot{\bar{x}}_2} \\ \frac{\partial \dot{x}_2}{\partial \bar{x}_1} & \frac{\partial \dot{x}_2}{\partial \dot{\bar{x}}_1} & \frac{\partial \dot{x}_2}{\partial \bar{x}_2} & \frac{\partial \dot{x}_2}{\partial \dot{\bar{x}}_2} \\ \frac{\partial \ddot{x}_2}{\partial \bar{x}_1} & \frac{\partial \ddot{x}_2}{\partial \dot{\bar{x}}_1} & \frac{\partial \ddot{x}_2}{\partial \bar{x}_2} & \frac{\partial \ddot{x}_2}{\partial \dot{\bar{x}}_2} \end{bmatrix} = \tag{23}$$

$$= \begin{bmatrix} 0 & 1 & 0 & 0 \\ -\alpha_1 - \alpha_2 - 3\left[\beta_1 \bar{x}_1^2 + \beta_2 (\bar{x}_2 - \bar{x}_1)^2\right] & -2(\zeta_1 + \zeta_2) & \alpha_2 + 3\beta_2 (\bar{x}_2 - \bar{x}_1)^2 & 2\zeta_2 \\ 0 & 0 & 0 & 1 \\ \frac{1}{\rho}\left[\alpha_2 + 3\beta_2 (\bar{x}_2 - \bar{x}_1)^2\right] & \frac{2\zeta_2}{\rho} & -\frac{1}{\rho}\left[\alpha_2 + 3\beta_2 (\bar{x}_2 - \bar{x}_1)^2\right] & -\frac{2\zeta_2}{\rho} \end{bmatrix}$$

The eigenvalues of $\mathbf{J}$ are determined by:

$$\det(\mathbf{J} - \lambda^{\mathrm{e}}\mathbf{I}) = 0 \tag{24}$$

The stability analysis can also be complemented by the point of view of the potential energy function of the system determined by:

$$\Psi(x_1, x_2) = \Psi_1 + \Psi_2 = \frac{1}{2}\alpha_1 x_1^2 + \frac{1}{4}\beta_1 x_1^4 + \frac{1}{2}\alpha_2 (x_2 - x_1)^2 + \frac{1}{4}\beta_2 (x_2 - x_1)^4 \tag{25}$$

Figure 2 shows some examples of possible equilibrium configurations of the system. Diamond shaped red dots represent unstable equilibrium points, while circular shaped blue dots represent stable equilibrium points. Energy levels associates with the potential energy function $\Psi(x_1, x_2)$ are depicted by the color scale; darker colors represent potential wells (low energy levels), while lighter colors represent higher energy levels.

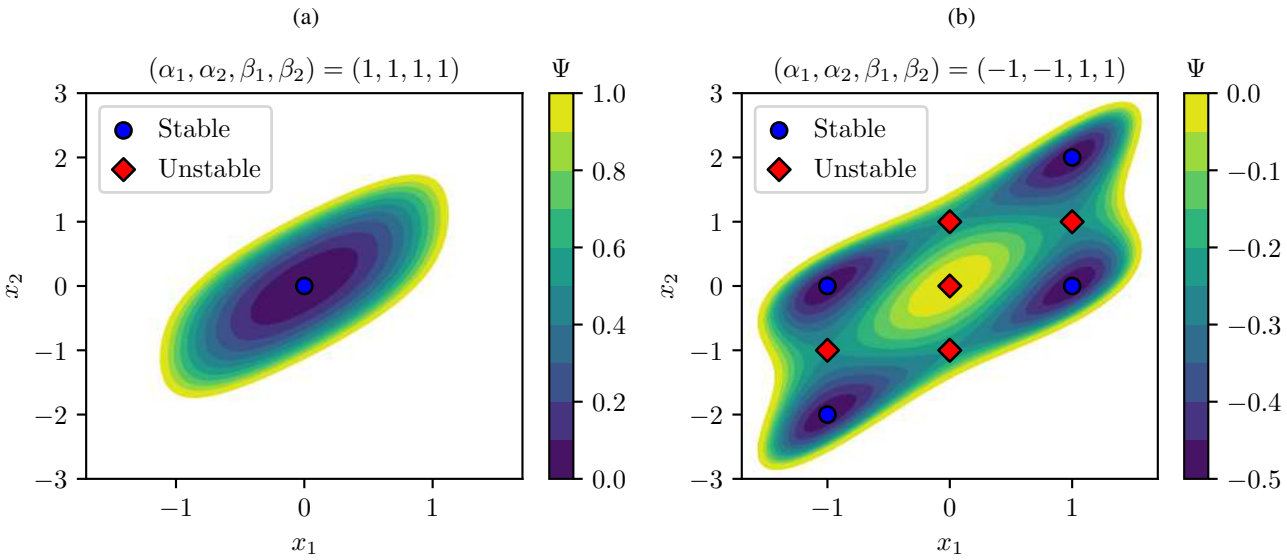

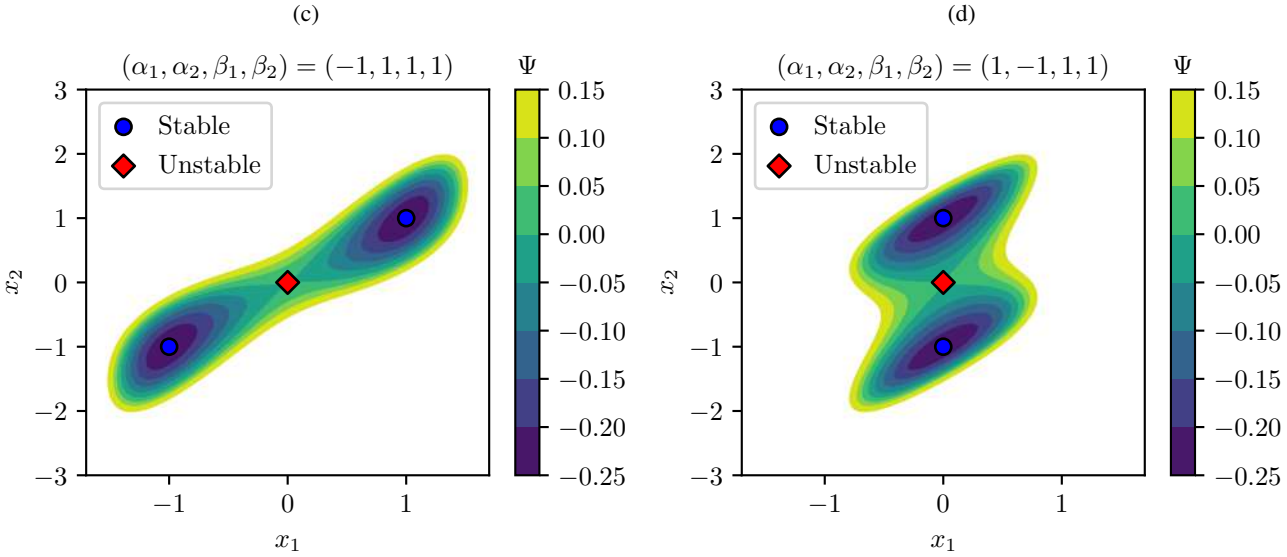

Figure 2: Equilibrium points and potential energy levels for different equilibrium configurations.

Summarizing, Table 1 shows all possible equilibrium configurations based on the 16 different combinations of α_1, α_2, β_1 and β_2 and the nature of stability for each point.

Table 1: Existence and nature of stability of equilibrium points according to the sign of dimensionless restoring force parameters.

α_1	α_2	β_1	β_2	EP_1	EP_2	EP_3	EP_4	EP_5	EP_6	EP_7	EP_8	EP_9	Total
+	+	+	+	Stable	✗	✗	✗	✗	✗	✗	✗	✗	1
−	−	−	−	Unst.	✗	✗	✗	✗	✗	✗	✗	✗	1
+	−	−	−	Unst.	✗	✗	Unst.	Unst.	✗	✗	✗	✗	3
+	+	−	−	Stable	Unst.	Unst.	Unst.	Unst.	Unst.	Unst.	Unst.	Unst.	9
+	+	+	−	Stable	Unst.	Unst.	✗	✗	✗	✗	✗	✗	3
−	+	+	+	Unst.	✗	✗	Stable	Stable	✗	✗	✗	✗	3
−	−	+	+	Unst.	Unst.	Unst.	Unst.	Unst.	Stable	Stable	Stable	Stable	9
−	−	−	+	Unst.	Unst.	Unst.	✗	✗	✗	✗	✗	✗	3
−	+	−	−	Unst.	Unst.	Unst.	✗	✗	✗	✗	✗	✗	3
−	−	+	−	Unst.	✗	✗	Unst.	Unst.	✗	✗	✗	✗	3
−	+	+	−	Unst.	Unst.	Unst.	Stable	Stable	Unst.	Unst.	Unst.	Unst.	9
+	−	+	−	Unst.	✗	✗	✗	✗	✗	✗	✗	✗	1
−	+	−	+	Unst.	✗	✗	✗	✗	✗	✗	✗	✗	1
+	−	−	+	Unst.	Stable	Stable	Unst.	Unst.	Unst.	Unst.	Unst.	Unst.	9
+	−	+	+	Unst.	Stable	Stable	✗	✗	✗	✗	✗	✗	3
+	+	−	+	Stable	✗	✗	Unst.	Unst.	✗	✗	✗	✗	3

4. NUMERICAL SIMULATIONS

In this section, numerical analyzes are performed employing fourth order Runge-Kutta integration method in order to solve the nonlinear system of equations $\dot{\mathbf{x}} = \mathbf{f}(\mathbf{x})$. A total of $n_p = 1000$ forcing periods were analyzed in each case. A stability configuration, depicted in Figure 2b, with 9 equilibrium points, being 4 stable and 5 unstable, is chosen to be the focus of this analysis. Dynamical response diagrams and Lyapunov exponent diagrams are built in order to map and identify different kinds of periodic and aperiodic attractors on the Ω and γ parameter domain. The procedure to classify different attractors is executed by comparing the magnitude of Lyapunov exponents and verifying the steady state Poincaré map of the time series in each case. Lyapunov exponent spectrum are examined, and then compared, in two distinct initial time stages $\tau_0 = 0$ and $\tau_0 = 0.75\tau_f$ (steady state), in order to ensure exponent convergence on cases that show long transient chaos orbits, where $\tau_f = 2\pi n_p/\Omega$ is the final time of integration. Results are classified based on the following attractors: Period-1, Period-2, Period-3, Period-4, Period-5, Period-6 or greater, Chaotic and Hyperchaotic. Each point in the diagrams is the result of a numerical integration starting from a specific initial condition. Table 2 summarizes the

parameters employed in all analyses and the stable equilibrium points based on the defined parameters.

Table 2: Parameters employed on the numerical analysis and its corresponding stable equilibrium points.

α_1	α_2	β_1	β_2	ζ_1	ζ_2	ρ	Ω	γ
-1	-1	1	1	0.025	0.025	1	$0.01 \longrightarrow 3$	$0.01 \longrightarrow 1$
EP_6	EP_7	EP_8	EP_9					
$(-1,0,-2,0)$	$(-1,0,0,0)$	$(1,0,0,0)$	$(1,0,2,0)$					

Figure 3 shows the dynamical response diagram and largest (λ_1) and second (λ_2) Lyapunov exponent diagrams for initial conditions based on EP_6 (Equation 19). In Fig. 3a, each color represents the classification of a different dynamical pattern of motion. In Fig. 3b and 3c rainbow colormap represents positive Lyapunov exponents, while grayscale colormap represents negative values of Lyapunov exponents. Results show complex patterns with the predominance of Period-1 (dark gray) and Hyperchaotic (dark red) responses. Period-2, period-3, period-6 and chaotic responses are present in certain specific areas of the diagram. On the other hand, period-5 patterns are not very robust, indicating certain difficulty to distinguish a safe zone to always find these types of responses. Period-4 responses are also difficult to find. The magnitude of positive λ_1 and λ_2 tend to be larger as Ω increases, to a point in which it starts to quickly decrease. Moreover, in certain zones, there is a decrease of the magnitude of λ_1 and λ_2 as γ decreases. An example of this behavior can be observed around $0.7 < \Omega < 1$, as hyperchaotic motion quickly turns into chaotic motion as λ_2 changes from positive to negative.

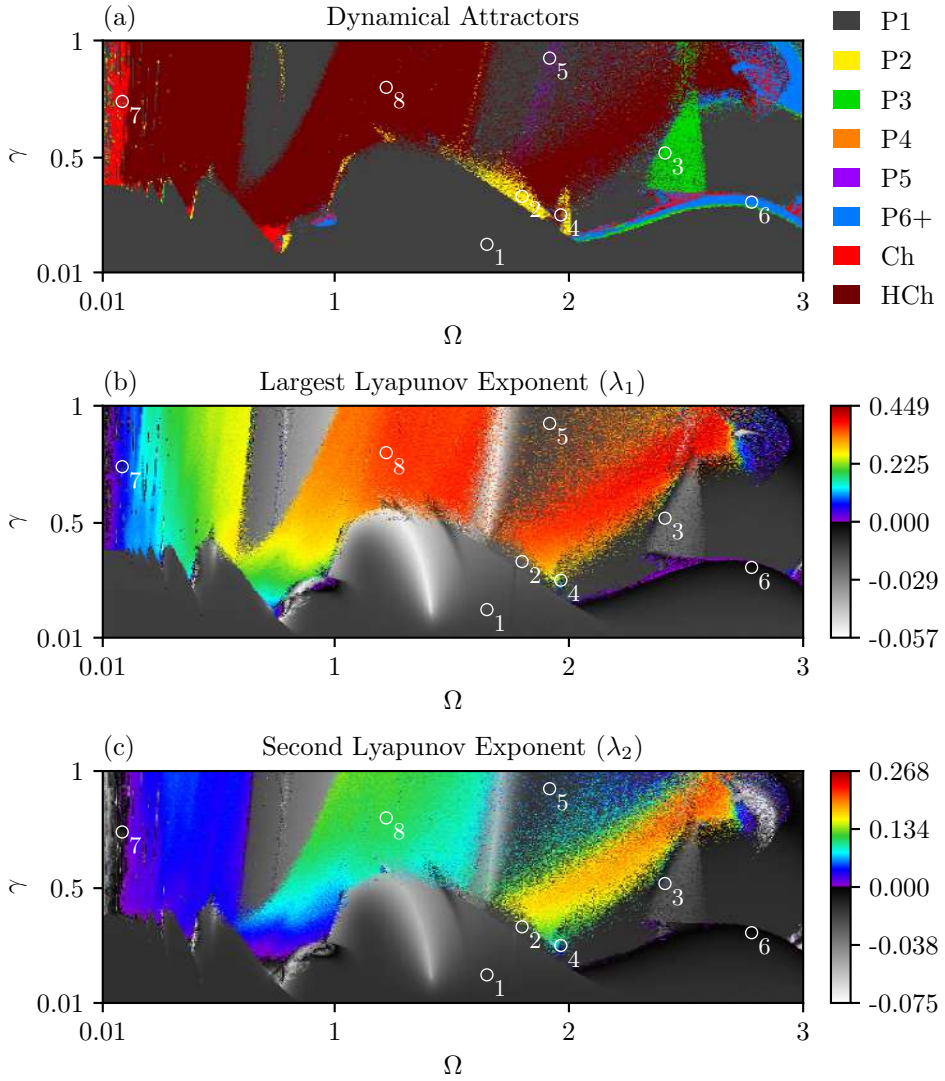

Figure 3: (a) Attractors based on the dynamical response of the system. P# (# $= 1, 2, 3, 4, 5, 6+$) stands for periodic motion, while Ch and HCh shows chaotic and hyperchaotic motion, respectively; (b) Largest Lyapunov exponent (λ_1) diagram; (c) Second Lyapunov exponent (λ_2) diagram.

Figure 3 highlights some points as an example of each dynamical response pattern of motion. x_1-$\dot{x}_1$, x_2-$\dot{x}_2$ and x_1-x_2 phase subspaces and Poincaré maps of these points are displayed in Figures 4 to 9 following the color of the dynamical response classification on the diagram. The titles in each phase space indicate the corresponding point in the dynamical response diagram.

Figure 4 represents the point (1) of a period-1 motion at $(\Omega, \gamma) = (1.65, 0.13)$ in the dynamical response diagram. This is an example of a dynamical behavior oscillating around EP_9.

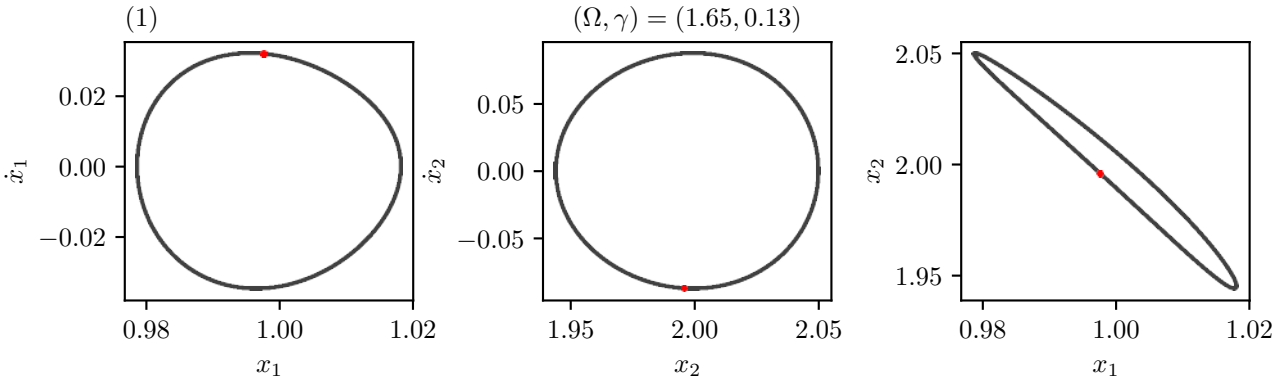

Figure 4: Phase subspaces and Poincaré maps of a period-1 motion oscillating around EP_9.

Figure 5 represents the point (2) of a period-2 motion at $(\Omega, \gamma) = (1.8, 0.335)$ in the dynamical response diagram. This illustrates an example of a dynamical behavior oscillating around EP_8. Observe that the equilibrium position of the system starts at EP_6 and the steady state response of these two last examples oscillates around different equilibrium positions (EP_9 and EP_8, respectively). These dynamical jumps occur due to the transient part of motion, showing different possibilities even for similar patterns of motion.

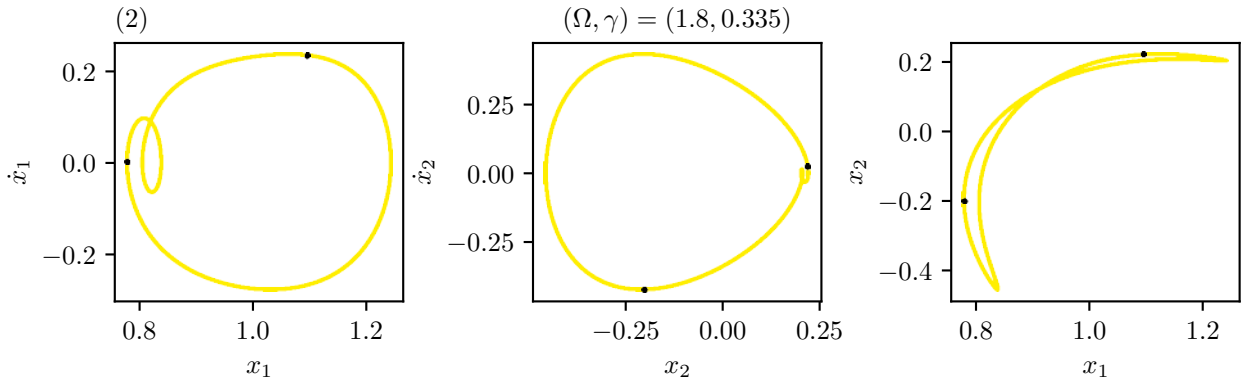

Figure 5: Phase subspaces and Poincaré maps of a period-2 motion oscillating around EP_8.

Figure 6 shows two different patterns of motion oscillating around EP_7. Green indicates period-3 motion and orange indicates period-4 motion. A similar jump phenomena occurs in the two degrees of freedom as the system starts at EP_6 and finishes oscillating around EP_7. It is also interesting to observe that, due to the scarcity of period-4 large areas in the dynamical response diagram in Figure 3, the need to specify more precise numbers with more decimal places in (Ω, γ) to find such behavior.

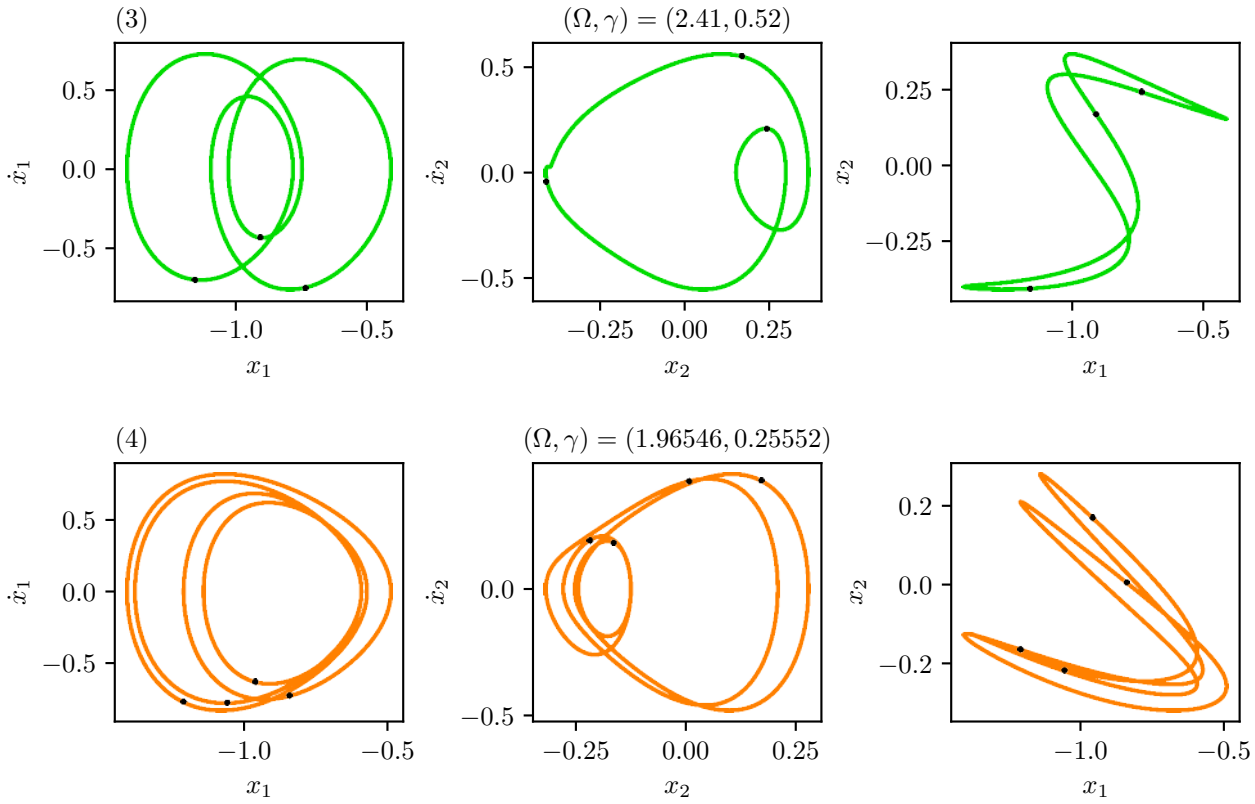

Figure 6: Phase subspaces and Poincaré maps of a period-3 and period-4 motion oscillating around EP_7.

Period-5 motion is illustrated in Figure 7. The non-robust nature of the period-5 zone in the dynamical response diagram justifies the need of more precise numbers to find an example of period-5 response. Phase subspace diagrams show that, in this case, the system oscillates around more than one stable equilibrium point (EP_7 and EP_8), visiting, at least, two potential energy wells in the process.

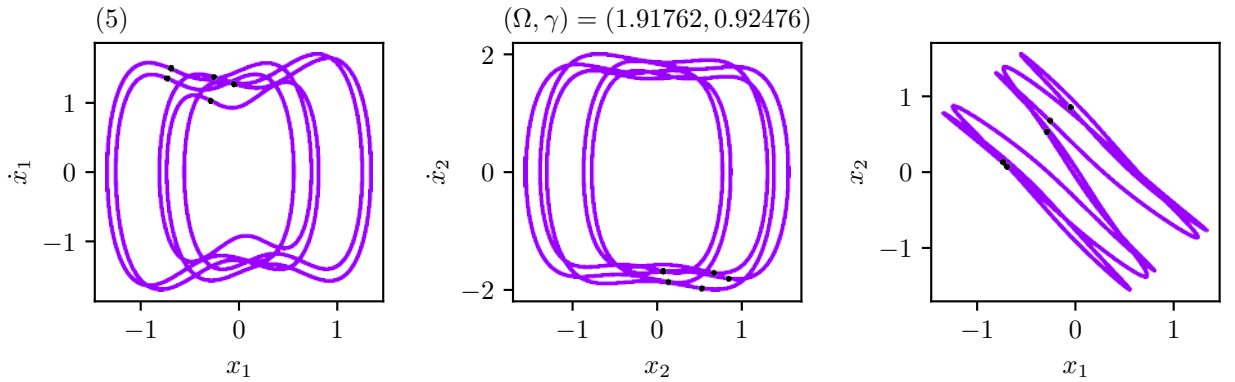

Figure 7: Phase subspaces and Poincaré maps of a period-5 motion oscillating around multiple equilibrium points.

An interesting behavior of a periodic motion with multiple periods is shown in Figure 8, represented by point (6) in the dynamical response diagram. A quick view points that this movement seems to be a period-1 response. Nevertheless, a closer look using a zoom shows that the Poincaré map has a star-like attractor indicating a multi-period periodic response. Despite the distinct form of the attractor, negative λ_1 ensures the motion periodicity.

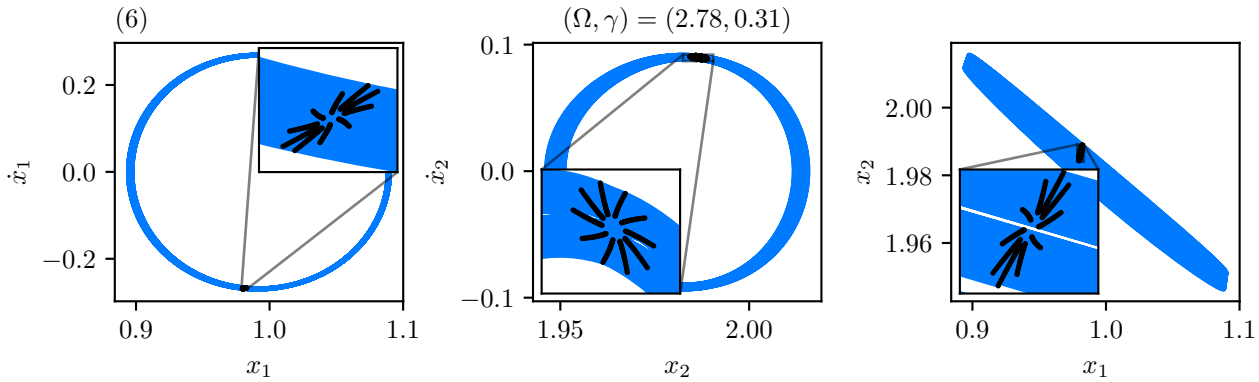

Figure 8: Phase subspaces and Poincaré maps of a periodic motion with multiple periods oscillating around EP_9.

Finally, Figure 9 shows examples of chaotic and hyperchaotic attractors, respectively, represented in points (7) and (8) in the dynamical response diagram. The two cases present strange attractors in the Poincaré map, however, chaotic attractors are represented by a positive larger Lyapunov exponent ($\lambda_1 > 0$) and a negative second Lyapunov exponent ($\lambda_2 < 0$). On the other hand, hyperchaotic attractor presents both $\lambda_1 > 0$ and $\lambda_2 > 0$. In other words, chaotic attractor presents only one instability direction, while hyperchaotic attractor presents two instability directions. It is also important to notice that the system visits all stable equilibrium points for these two cases. Chaotic case (7) presents only one equilibrium point that is not visited, the unstable one $EP_1 = (\bar{x}_1, \dot{\bar{x}}_1, \bar{x}_2, \dot{\bar{x}}_2) = (0, 0, 0, 0)$. On the other hand, hyperchaotic case (8) visits all stable and unstable equilibrium points.

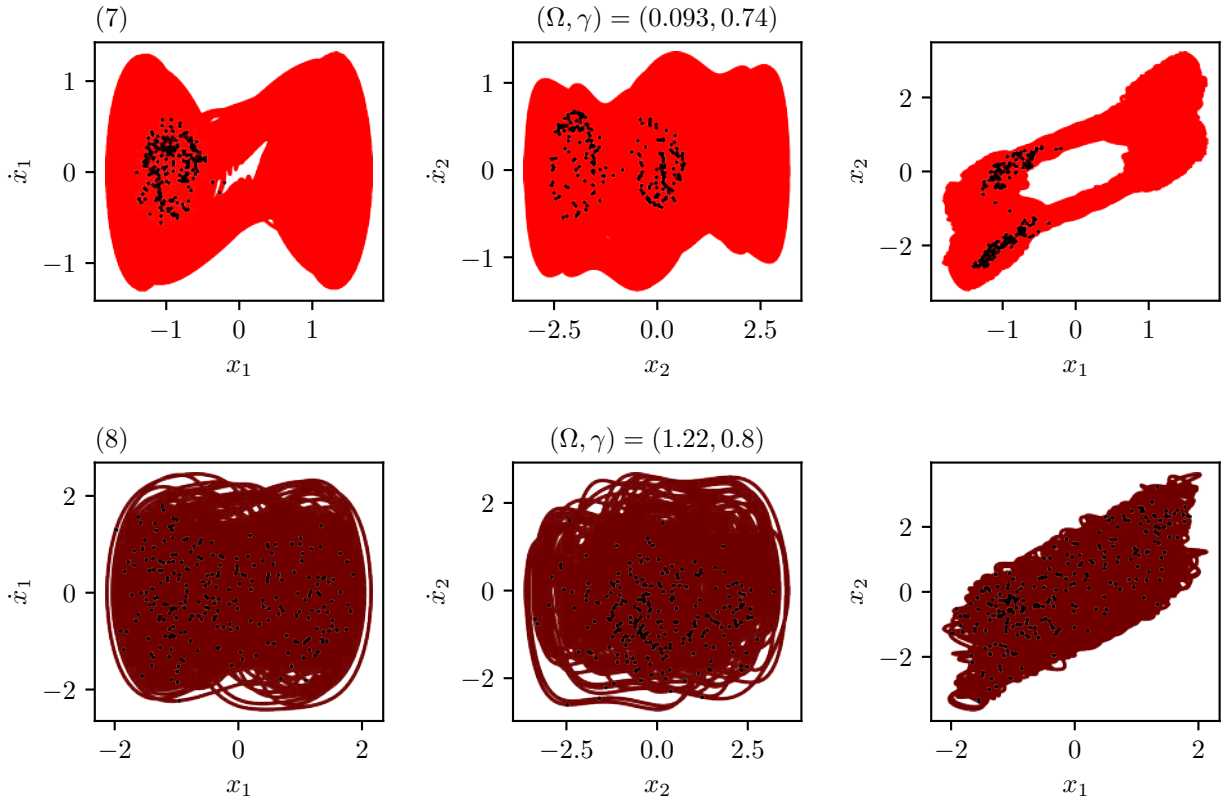

Figure 9: Phase subspaces ans Poincaré maps of a Chaotic and Hyperchaotic motions oscillating around all stable equilibrium points.

Another observable difference between the chaotic and hyperchaotic attractors can be highlighted by integrating the nonlinear system with more forcing periods, resulting in more points in the Poincaré Map. Figure 10 shows that chaotic attractor has a fractal characteristic, while the hyperchaotic attractor has a messier structure.

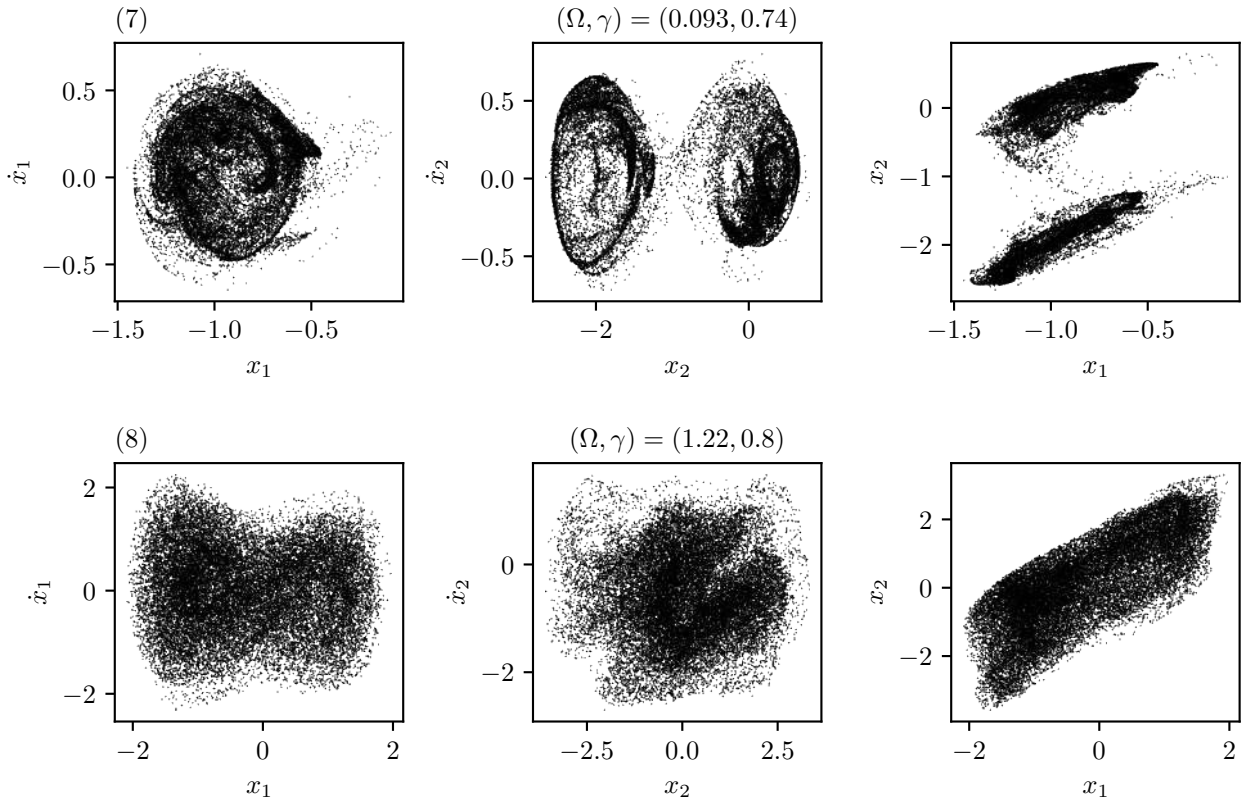

Figure 10: Poincaré maps of a Chaotic and Hyperchaotic attractors for $n_p = 10^5$ forcing periods.

5. CONCLUSIONS

This work addresses a numerical analysis of a two-degree of freedom Duffing Oscillator in order to map different kinds of dynamical responses of the system. Stability analysis shows a variety of 16 equilibrium configurations depending on the combination of the stiffness parameters α_1, α_2, β_1, β_2. Each equilibrium configuration exhibits a certain quantity of equilibrium points: 1, 3 or 9, but each one singular. An equilibrium configuration of 9 equilibrium points was chosen to be the focus of the numerical analysis as it presents more complexity exhibiting 4 stable and 5 unstable equilibrium points. Fourth order Runge-Kutta integration method was employed in order to solve the nonlinear system. A procedure to classify different dynamical attractors representing distinct types of periodic and aperiodic dynamical responses was executed by comparing the magnitude of Lyapunov Exponents and verifying the steady state Poincaré map of the time series. This procedure was done several times with different external forcing parameters to build dynamical response and Lyapunov exponent diagrams in order to map the system's behaviors in the Ω (frequency) and γ (amplitude) domain. Results show complex behaviors associated with the predominance of period-1 and hyperchaotic attractors. In addition, specific zones of period-2, period-3, period-6 or greater and chaotic are found presenting a robust occurrence in the map. On the other hand, period-4 and period-5 areas exist but are not robust enough to safely distinct a zone for these behaviors, at least for the range of parameters analyzed.

6. ACKNOWLEDGEMENTS

The authors would like to acknowledge the support of the Brazilian Research Agencies CNPq, CAPES and FAPERJ.

7. REFERENCES

Costa, L., Loureiro da Silva Monteiro, L. and Savi, M., 2019. "A Parametric Analysis of the Nonlinear Dynamics of a Duffing Oscillator". In *Proceedings of the 25th International Congress of Mechanical Engineering*. ABCM, pp. 3–7. doi:10.26678/ABCM.COBEM2019.COB2019-0258.

Costa, L.G., Monteiro, L.L.d.S., Pacheco, P.M.C.L. and Savi, M.A., 2021. "A parametric analysis of the nonlinear dynamics of bistable vibration-based piezoelectric energy harvesters". *Journal of Intelligent Material Systems and Structures*, Vol. 32, No. 7, pp. 699–723. ISSN 15308138. doi:10.1177/1045389X20963188.

Duffing, G., 1918. *Erzwungene Schwingungen bei veränderlicher Eigenfrequenz und ihre technische Bedeutung*. Vieweg.

Erturk, A. and Inman, D.J., 2011. "Broadband piezoelectric power generation on high-energy orbits of the bistable Duffing

oscillator with electromechanical coupling". *Journal of Sound and Vibration*, Vol. 330, No. 10, pp. 2339–2353. ISSN 0022-460X. doi:https://doi.org/10.1016/j.jsv.2010.11.018.

Fouda, J.A.E., Bodo, B., Djeufa, G.M. and Sabat, S.L., 2016. "Experimental chaos detection in the Duffing oscillator". *Communications in Nonlinear Science and Numerical Simulation*, Vol. 33, pp. 259–269. ISSN 10075704. doi: 10.1016/j.cnsns.2015.09.011.

Gottwald, J., Virgin, L. and Dowell, E., 1992. "Experimental mimicry of Duffing's equation". *Journal of Sound and Vibration*, Vol. 158, No. 3, pp. 447–467. ISSN 0022460X. doi:10.1016/0022-460X(92)90419-X.

Hikihara, T. and Kawagoshi, T., 1996. "An experimental study on stabilization of unstable periodic motion in magneto-elastic chaos". *Physics Letters, Section A: General, Atomic and Solid State Physics*, Vol. 211, No. 1, pp. 29–36. ISSN 03759601. doi:10.1016/0375-9601(95)00925-6.

Kenfack, A., 2003. "Bifurcation structure of two coupled periodically driven double-well Duffing oscillators". *Chaos, Solitons and Fractals*, Vol. 15, No. 2, pp. 205–218. ISSN 09600779. doi:10.1016/S0960-0779(01)00250-8.

Masana, R. and Daqaq, M.F., 2011. "Relative performance of a vibratory energy harvester in mono- and bi-stable potentials". *Journal of Sound and Vibration*, Vol. 330, No. 24, pp. 6036–6052. ISSN 0022-460X. doi: https://doi.org/10.1016/j.jsv.2011.07.031.

Moon, F.C. and Holmes, P.J., 1979. "A magnetoelastic strange attractor". *Journal of Sound and Vibration*, Vol. 65, No. 2, pp. 275–296. ISSN 0022-460X. doi:https://doi.org/10.1016/0022-460X(79)90520-0.

Musielak, D.E., Musielak, Z.E. and Benner, J.W., 2005. "Chaos and routes to chaos in coupled Duffing oscillators with multiple degrees of freedom". *Chaos, Solitons and Fractals*, Vol. 24, No. 4, pp. 907–922. ISSN 09600779. doi: 10.1016/j.chaos.2004.09.119.

Natsiavas, S. and Hagler, L.B., 1991. "Modal interaction and bifurcations in two degree of freedom duffing oscillators". *Nonlinear Dynamics*, Vol. 2, No. 6, pp. 405–417. ISSN 0924090X. doi:10.1007/BF00045436.

Paula, A.S.D., Inman, D.J. and Savi, M.A., 2015. "Energy harvesting in a nonlinear piezomagnetoelastic beam subjected to random excitation". *Mechanical Systems and Signal Processing*, Vol. 54-55, pp. 405–416. ISSN 0888-3270. doi: https://doi.org/10.1016/j.ymssp.2014.08.020.

Savi, M.A. and Pacheco, P.M., 2002. "Chaos in a two-degree of freedom duffing oscillator". *Revista Brasileira de Ciencias Mecanicas/Journal of the Brazilian Society of Mechanical Sciences*, Vol. 24, No. 2, pp. 115–121. ISSN 01007386. doi:10.1590/S0100-73862002000200006.

Savi, M., 2017. *Dinâmica Não-linear E Caos*. E-papers. ISBN 9788576505549.

Tam, J.I. and Holmes, P., 2014. "Revisiting a magneto-elastic strange attractor". *Journal of Sound and Vibration*, Vol. 333, No. 6, pp. 1767–1780. ISSN 10958568. doi:10.1016/j.jsv.2013.11.022.

Wolf, A., Swift, J.B., Swinney, H.L. and Vastano, J.A., 1985. "Determining Lyapunov exponents from a time series". *Physica D*, Vol. 16, No. 3, pp. 285–317. ISSN 01672789. doi:10.1016/0167-2789(85)90011-9.

Zaher, A.A., 2018. "Duffing oscillators for secure communication". *Computers and Electrical Engineering*, Vol. 71, No. July, pp. 77–92. ISSN 00457906. doi:10.1016/j.compeleceng.2018.07.005.

Zeni, A.R. and Gallas, J.A., 1995. "Lyapunov exponents for a Duffing oscillator". *Physica D: Nonlinear Phenomena*, Vol. 89, No. 1-2, pp. 71–82. ISSN 01672789. doi:10.1016/0167-2789(95)00215-4.

8. RESPONSIBILITY NOTICE

The authors are solely responsible for the printed material included in this paper.